

Carrier lifetimes in high-lifetime silicon wafers and solar cells measured by photoexcited muon spin spectroscopy

Cite as: J. Appl. Phys. 132, 065704 (2022); doi: 10.1063/5.0099492

Submitted: 17 May 2022 · Accepted: 14 July 2022 ·

Published Online: 12 August 2022



View Online



Export Citation



CrossMark

J. D. Murphy,^{1,a)} N. E. Grant,¹ S. L. Pain,¹ T. Nieuwelt,^{1,2,3} A. Wratten,¹ E. Khorani,¹ V. P. Markevich,⁴ A. R. Peaker,⁴ P. P. Altermatt,⁵ J. S. Lord,⁶ and K. Yokoyama⁶

AFFILIATIONS

¹School of Engineering, University of Warwick, Coventry CV4 7AL, United Kingdom

²Fraunhofer Institute for Solar Energy Systems ISE, Heidenhofstraße 2, 79110 Freiburg, Germany

³Institute for Sustainable Systems Engineering, University of Freiburg, Emmy-Noether-Straße 2, 79110 Freiburg, Germany

⁴Department of Electrical and Electronic Engineering, University of Manchester, Manchester M13 9PL, United Kingdom

⁵Trina Solar Limited, State Key Laboratory for PV Science and Technology (SKL), Changzhou 213031, China

⁶ISIS Neutron and Muon Source, STFC Rutherford Appleton Laboratory, Didcot, OX11 0QX, United Kingdom

^{a)}Author to whom correspondence should be addressed: john.d.murphy@warwick.ac.uk

ABSTRACT

Photoexcited muon spin spectroscopy (photo- μ SR) is used to study excess charge carrier lifetimes in silicon. Experiments are performed on silicon wafers with very high bulk lifetimes with the surface passivation conditions intentionally modified to control the effective lifetime. When the effective lifetime is low ($<500\ \mu\text{s}$), implanting the muons to different depths enables the reliable measurement of carrier lifetime as a function of distance from a surface. It is also demonstrated that the photo- μ SR technique can measure effective carrier lifetimes in completed commercial gallium doped silicon passivated emitter and rear cell devices, with results validated with harmonically modulated photoluminescence imaging. It is discovered, however, that prolonged muon irradiation of samples with very long effective lifetimes ($>10\ \text{ms}$) results in detectable degradation of the measured lifetime. Re-passivation of degraded samples with a temporary room temperature superacid-based passivation scheme demonstrates that degradation occurs in the silicon bulk. Deep-level transient spectroscopy measurements reveal the existence of several defect-related traps near the muon-exposed surface in concentrations of order $10^{10}\ \text{cm}^{-3}$ that are not present near the surface not exposed to muons. In contrast to the common perception of the μ SR technique, our results demonstrate that muons are not inert probes and that beam-induced recombination activity modifies the bulk lifetime significantly in samples with high effective carrier lifetimes.

© 2022 Author(s). All article content, except where otherwise noted, is licensed under a Creative Commons Attribution (CC BY) license (<http://creativecommons.org/licenses/by/4.0/>). <https://doi.org/10.1063/5.0099492>

I. INTRODUCTION

Excess charge carrier lifetime (henceforth just “lifetime”) is a key property of semiconductor materials, which is often crucial for the performance of electronic devices, such as solar cells and bipolar transistors. There are well-established methods to measure lifetime, such as photoconductance decay (PCD) and modulated photoluminescence (PL).

It has recently been demonstrated that lifetime measurements can be made by photoexcited muon spin spectroscopy (photo- μ SR)

using the high-power pulsed laser system on the high magnetic field muon spectrometer (HiFi) at ISIS.^{1–3} This technique involves exciting carriers with a laser light pulse shortly followed by the implantation of 4 MeV positive muons (μ^+), measuring the emitted decay positron and finally obtaining the muon spin asymmetry time spectrum. The spin relaxation processes are driven by a complex network of transitions between states, as discussed previously in Ref. 1 and references therein. The precise details of the transition channels are beyond the scope of this paper, so we only

provide an outline of the key mechanisms here. The spin-polarized positive muons capture electrons to form muonium “atoms” ($\text{Mu} = \mu^+ + e^-$). Illumination creates electron-hole pairs in the semiconductor, which then start charge exchange interactions with Mu atoms. One important interaction occurs when photogenerated holes recombine with the bound electron in the Mu, freeing up μ^+ , hence enabling the capture of another electron of either spin state. Other interactions including the formation of negatively charged Mu by μ^+ capturing two electrons and its subsequent ionization by a hole are also possible. Ultimately, muons with an opposite electronic spin are depolarized via hyperfine interaction ($\sim\text{GHz}$), whereas muons with a parallel electronic spin can maintain their spin polarization. The net result of the complex network of processes is spin depolarization of Mu, the rate of which (λ) is proportional to the excess carrier density (Δn) in the semiconductor and can be determined from the relaxation of a μSR time spectrum as described in Ref. 1. By changing the time interval between the laser pulse and the muon pulse (Δt), a carrier lifetime spectrum can be determined from measurements of λ . Photo- μSR has been demonstrated as a technique to measure carrier lifetime in silicon^{1,3} and germanium.²

The photo- μSR technique allows lifetime to be measured as a function of depth within a sample, as the implantation depth of the muon probe can be modified by inserting degraders into the beam path.³ Depth-dependent lifetime is particularly important for high-purity bulk indirect gap semiconductors (e.g., Si, Ge), for which surface recombination can significantly reduce the effective lifetime toward the surface. Previous work using photo- μSR has measured lifetimes in unpassivated samples^{1,2} or in samples with partially hydrogen-terminated surface states following an HF dip,³ so the surface recombination velocities for the samples studied to date are a lot higher than those which can be achieved with dielectric surface passivation (see a recent review⁴). Atomic layer deposition (ALD) is a widely used technique for the production of nanometer-scale thin films (see Ref. 5 for a review). Many materials grown via ALD are able to passivate silicon surfaces very effectively, with Al_2O_3 widely used,⁶ and other materials such as HfO_2 ⁷ having potential. In this study, we use high-lifetime silicon samples passivated with Al_2O_3 and HfO_2 with a view to establishing the limits of the photo- μSR lifetime measurement technique.

Another aim of this study is to demonstrate new uses of the photo- μSR technique. We first demonstrate that photo- μSR can be applied to thin ($120\text{--}130\,\mu\text{m}$) samples, which means the technique can be applied to wafers used for commercial solar cells. Second,

given that muons easily penetrate any surface passivation layers or diffused/metallized regions, we demonstrate that the technique can be applied to completed commercial solar cell devices. Lifetime measurements on such structures with PCD approaches are more restricted. Application of the harmonically modulated PL technique^{8,9} offers a pathway to lifetime measurements on such samples. We use photo- μSR to measure effective lifetime in passivated emitter and rear cell (PERC) solar cells, which are now industry standard (see Ref. 10 for a review), and verify the results against those from harmonically modulated PL.

II. EXPERIMENTAL METHODS

A. Sample preparation and pre-characterization

Experiments were performed on silicon wafer samples and on completed PERC silicon solar cells. Wafer samples (approximately $5 \times 5\,\text{cm}^2$) were made from very high lifetime ($>20\,\text{ms}$) substrates and were passivated with thin-film dielectrics grown by ALD to reduce surface recombination. Different passivation conditions were used to produce samples with different effective lifetimes. Al_2O_3 passivation was applied to $2000\,\Omega\text{ cm}$ *n*-type Czochralski silicon wafers ($\sim 750\,\mu\text{m}$ thick) and HfO_2 passivation was applied to $5\,\Omega\text{ cm}$ *n*-type Czochralski silicon wafers ($\sim 130\,\mu\text{m}$ thick). Sample properties are given in Table I.

Prior to ALD passivation, samples were subjected to a wet chemical cleaning sequence: (i) 10 min in SC1 mix [“standard clean 1,” comprising H_2O , H_2O_2 (30%), and NH_4OH (30%) in a 5:1:1 ratio] at $\sim 80^\circ\text{C}$; (ii) a 2% HF dip; (iii) an etch in 25% tetramethylammonium hydroxide (TMAH) for 10 min at $\sim 80^\circ\text{C}$; (iv) a 2% HF dip; (v) 10 min in an SC2 mix [“standard clean 2,” comprised of H_2O , H_2O_2 (30%), and HCl (50%) in a 5:1:1 ratio] at $\sim 80^\circ\text{C}$; and then (vi) a dip in HF (2%) for 10 s before being pulled dry (without any water rinsing). ALD was performed in a Veeco Fiji G2 system featuring an external load lock. Aluminum oxide was deposited at 200°C using a plasma O_2 source and a trimethylaluminum precursor for 200 cycles to give films of $\sim 20\text{--}25\,\text{nm}$ thickness. For two-sided passivated samples, the sample was turned over and the same ALD process was applied to the other side. One sample was passivated with HfO_2 on both sides with the deposition performed using 200 ALD cycles using a tetrakis(dimethylamido) hafnium precursor at 200°C with O_2 plasma resulting in about 25 nm layer thickness. A 30 min postdeposition anneal was performed in a quartz tube furnace in air, with the temperature chosen in the range $350\text{--}450^\circ\text{C}$, as specified in Table I. Transient

TABLE I. Properties of the passivated silicon wafer sample set used and muon exposure times. All these samples were *n*-type.

| Sample | Resistivity ($\Omega\text{ cm}$) | Doping (cm^{-3}) | Thickness (μm) | Passivation | Sides | Activation annealing temperature ($^\circ\text{C}$) | Initial τ_{PCD} at $\Delta n = 10^{15}\,\text{cm}^{-3}$ (ms) | Muon exposure |
|--------|---------------------------------------|--------------------------------|--------------------------------|-------------------------|-------|---|--|--|
| A | 2000 | 2.2×10^{12} | 750 | Al_2O_3 | One | 450 | 0.32 | 37.8 h (unpassivated side) + 13.3 h (passivated side) = 51.1 h (total) |
| B | 2000 | 2.2×10^{12} | 750 | Al_2O_3 | Two | 350 | 4.66 | 52.0 h (one side) |
| C | 2000 | 2.2×10^{12} | 750 | Al_2O_3 | Two | 400 | 22.57 | 39.2 h (one side) |
| D | 5 | 9.1×10^{14} | 130 | HfO_2 | Two | 400 | 1.38 | 18.2 h (one side) |

PCD was used to measure effective lifetimes with values measured using this technique referred to as τ_{PCD} . Transient PCD was measured with a Sinton WCT-120 lifetime tester at approximately 30 °C and τ_{PCD} prior to any photo- μ SR measurements are plotted as a function of excess carrier density (Δn) in Fig. 1(a), with values at $\Delta n = 10^{15} \text{ cm}^{-3}$ given in Table I.

Three PERC solar cells made from gallium doped silicon substrates with different resistivities were also studied. They were produced on usual commercial fabrication lines at Trina Solar at the time of production in December 2020, with an overview of the technology given in Ref. 11. Uncertified cell properties are stated in Table II. The finished $\sim 150 \mu\text{m}$ thick cells were cleaved into $5 \times 5 \text{ cm}^2$ pieces for handling purposes.

B. Photoexcited muon spin spectroscopy

Photo- μ SR lifetime experiments were carried out at 300 K using the high-power pulsed laser system¹² on the high magnetic field muon spectrometer (HiFi)¹³ at the ISIS Neutron and Muon Source at the STFC Rutherford Appleton Laboratory using a technique developed by Yokoyama *et al.*¹⁻³ A detailed explanation of the effective lifetime evaluation can be found in Ref. 1. The measurement configuration used here is shown in Fig. 1(b) with the implantation depth of the 4 MeV muons being controlled by inserting metal sheet degraders into the beam path, as discussed in Ref. 3. The degrader-covered muon exposed side is shown in Fig. 1(c), and Fig. 1(d) shows the side where laser illumination using the Nd:YAG fundamental (1064 nm) as pump laser light through an $\sim 3 \text{ cm}$ aperture is used to excite excess charge carriers. The 15 ns duration laser pulse energy was typically 2 mJ/pulse with a beam size of 8 cm^2 , covering the entire aperture. This corresponds to approximately $8.5 \times 10^{16} \text{ photons/cm}^2$, with the number of electron-hole pairs created dependent on the sample thickness due to the weak absorption of the 1064 nm wavelength.

Different degraders were used to control the muon implantation depth within the samples, with the combinations used shown in Table III. The distribution profiles were simulated using a Monte Carlo simulation package ("musrSim"¹⁴) using the known muon momentum and the thickness and density of degrader materials. Distributions are referred to by their peak depth relative to an incident surface and when fitted with Gaussian peaks had a full width at half maximum (FWHM) of $140 \pm 2 \mu\text{m}$. Calculated peak depths and muon energies at the sample surface are given in Table III. Five different degrader configurations were used for $\sim 750 \mu\text{m}$ thick wafer samples with the simulated depth profiles shown in Fig. 2(a). Thin samples (HfO₂ passivated wafers and PERC solar cells) were measured at a single depth. In the thin samples, the muon distribution spans across the whole sample depth, as shown in Fig. 4(a). Muons outside the sample are stopped either in the degraders or in air (the instrument was in atmosphere for all measurements), and these contribute to the muon asymmetry merely as a flat background.

The timing of the laser and muon pulses (separated by Δt) is shown schematically in Fig. 1(e), with repetition rate of the laser and muon pulses being 25 Hz and (pseudo-)50 Hz, respectively.¹² The laser repetition rate can, however, be further reduced to $25/n$ (integer $n > 1$) Hz for measurements with longer time constants,

which was necessary for the measurements on samples with very long effective lifetimes. Photo- μ SR experiments at ISIS generally run on a "period" mode¹⁵ in which positron data are recorded in different groups ("periods") according to the external stimulus applied. In these measurements, typically two periods were used, alternately "laser off" and "laser on" with the laser running at 25 Hz. In this experiment, each period collected for 5 million decay positron events (MEv) for a total of 10 MEv in the run. However, for two-sided Al₂O₃ passivated samples, the lifetime was very long, so the laser repetition rate was reduced to 12.5 Hz to ensure injected carriers completely died out before the next laser pump pulse. For these samples, there were four periods ($\Delta t + 0 \text{ ms}$, $\Delta t + 20 \text{ ms}$, $\Delta t + 40 \text{ ms}$, and $\Delta t + 60 \text{ ms}$, with the last serving as "laser off"). Long-lifetime samples, therefore, required 20 MEv per run to get equivalent statistics.

The effective lifetime measurement in photo- μ SR requires a slow intrinsic relaxation in the dark μ SR time spectrum (normally $< 1 \mu\text{s}^{-1}$) to measure a relaxation rate induced by carrier injection accurately. To achieve this, a longitudinal magnetic field (its vector parallel to initial muon spin) is applied to the sample. Under higher fields, the Mu hyperfine interaction is more decoupled, making the intrinsic relaxation rate lower. However, this makes the muon signal less sensitive to the charge exchange interaction with injected carriers. A higher level of carrier injection is, therefore, required when a larger field is applied, which is achieved by increasing the laser power by changing optical filter configurations. For most experiments, a small field of 10 mT was applied; however, significant dark relaxation was found in the HfO₂ and one-sided Al₂O₃ passivated samples (samples D and A, respectively) so a larger field of 0.3 T was applied in these cases.

Each sample underwent a series of photo- μ SR measurements, with measurements often made with a range of degrader configurations to vary the muon implantation depth. Some samples were measured both ways round. Muon exposure times varied considerably between samples with estimates of the total muon exposure duration given in Table I for wafer samples and in Table II for PERC cells.

C. Post-muon exposure characterization

After muon exposure, the samples were characterized again by PCD effective lifetime measurements. PL imaging and deep-level transient spectroscopy (DLTS) were used to investigate the degradation effects occurring after prolonged exposure. Uncalibrated room temperature photoluminescence imaging using a 650 nm LED array and a silicon CCD camera was performed at the University of Warwick for qualitative assessment of sample quality. Subsequently, harmonically modulated effective lifetime measurements were performed on some of the samples at 298 K with a *modulum* tool at Fraunhofer ISE, resulting in quantitative lifetime-calibrated luminescence images of the samples, as well as plots of effective lifetime from PL (denoted by τ_{PL}) against Δn .^{8,9}

After PL characterization, the passivation layer was removed from the Al₂O₃ passivated samples and the samples were re-passivated using a superacid-based technique using bis(trifluoromethane)sulfonimide (TFSI),^{16,17} which gives a level of temporary surface passivation similar to dielectric thin films.¹⁸

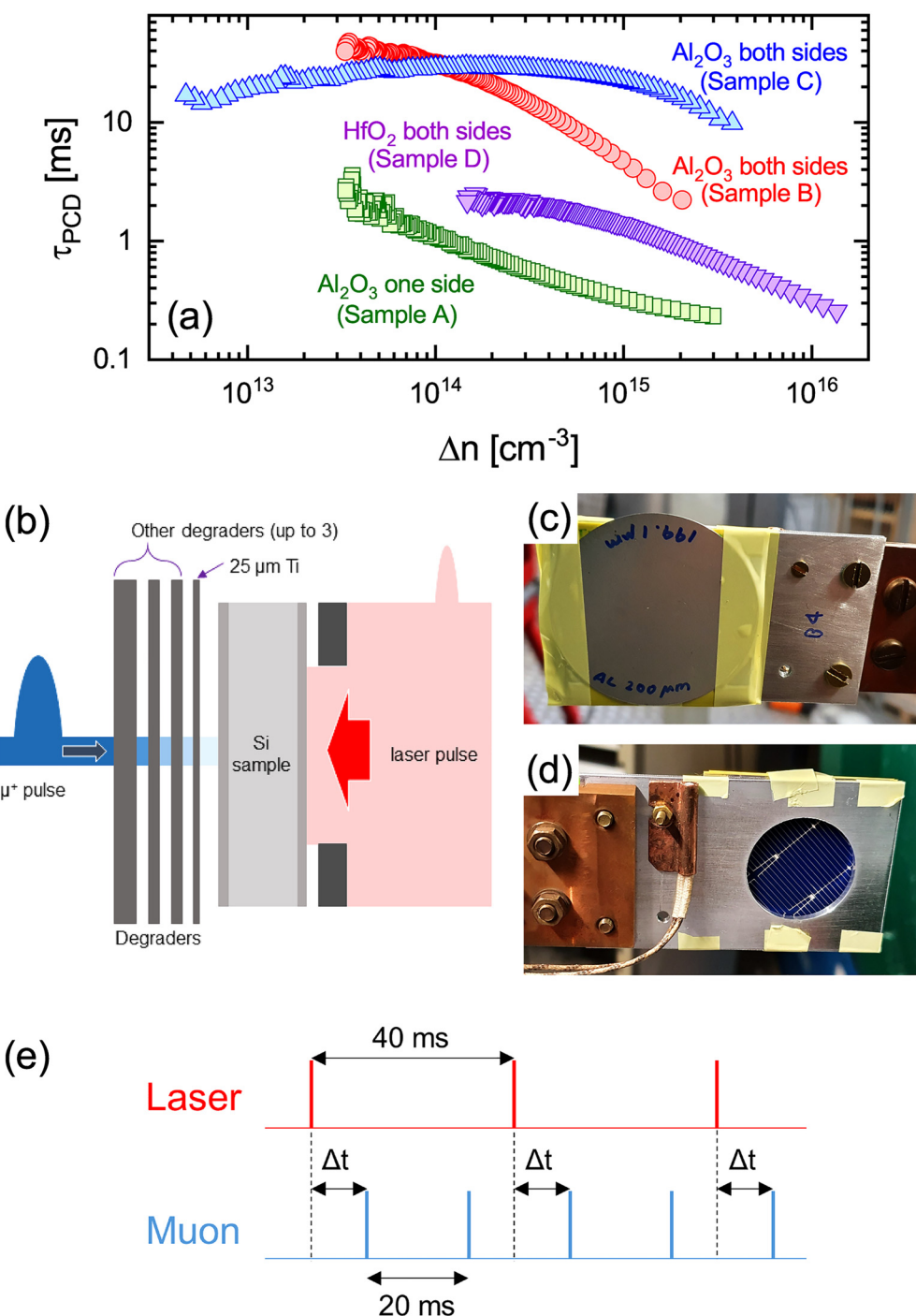


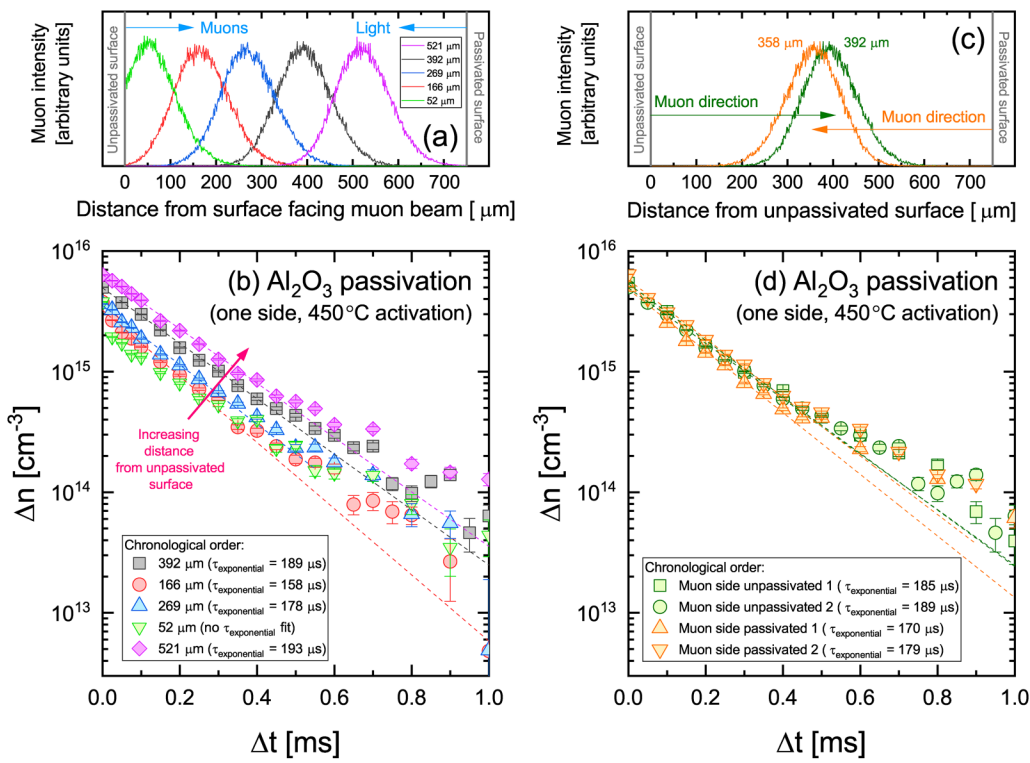
FIG. 1. (a) Effective lifetime from transient PCD vs excess carrier density measured prior to muon exposure for samples passivated on one or both sides with Al_2O_3 ($750 \mu\text{m}$ thick wafers) or on both sides with HfO_2 ($130 \mu\text{m}$ thick wafer), with properties given in Table I. (b) A schematic to show the measurement configuration for photo- μ SR lifetime measurements with degrader configurations given in Table III. (c) A photograph of the degraders covering the sample from the muon-exposed side. (d) A photograph of the light-exposed side of a PERC device in the sample holder (diameter of hole is $\sim 3 \text{ cm}$). (e) A timing diagram of the laser and muon pulses, with Δt being the time after the laser pulse at which the next muon pulse arrives. This diagram shows the standard laser pulse frequency of 25 Hz used for most photo- μ SR experiments (except those with very long lifetimes).

TABLE II. Properties of the Ga doped silicon PERC solar cells studied and muon exposure times.

| Substrate resistivity ($\Omega \text{ cm}$) | Substrate doping (cm^{-3}) | Efficiency (%) | Open circuit voltage (mV) | Muon exposure |
|---|---------------------------------------|----------------|---------------------------|---|
| 0.3 | 6.1×10^{16} | 22.81 | 678.3 | 5.5 h (rear) |
| 0.6 | 2.7×10^{16} | 22.94 | 680.6 | 20.7 h (rear) + 14.1 h (front) = 34.8 h (total) |
| 1 | 1.5×10^{16} | 23.13 | 683.8 | 7.3 h (rear) |

TABLE III. Degrader configurations used for photo- μ SR experiments, with muon peak depths and energies at the sample surface calculated by Monte Carlo simulation.

| Used for | Peak depth (μm) | Degrader materials | Muon energy at sample surface (MeV) |
|---------------------------------------|------------------------------|--|-------------------------------------|
| Thick samples | 521 | 25 μm Ti | 3.29 ± 0.20 |
| | 392 | 25 + 75 μm Ti | 2.82 ± 0.23 |
| | 269 | 25 + 75 + 108 μm Ti | 2.29 ± 0.28 |
| | 166 | 25 + 75 μm Ti + 108 μm Al | 1.74 ± 0.36 |
| | 52 | 25 + 75 μm Ti + 300 μm Al | 1.05 ± 0.42 |
| | 79 | 25 + 75 + 50 μm Ti + 200 μm Al | 1.20 ± 0.43 |
| Thin samples (including PERC devices) | | | |

**FIG. 2.** Results of two photo- μ SR experiments on a silicon wafer sample (750 μm thick) passivated with Al_2O_3 on only one side (sample A). The first experiment studied the depth dependence of the lifetime with simulated muon depths profile plotted in (a) and the corresponding lifetime spectra plotted in (b) with experiments performed in the order of the legend. The second studied the stability of the measurement and the impact of sample orientation. The sample was measured with the unpassivated side facing the muon beam before it was flipped so the passivated side faced the muon beam, with the muon depth profiles shown in (c). The lifetime spectra shown in (d) are for two repeat measurements on each side in the order of the legend.

Importantly, the superacid-based approach does not require the sample to be heated above 80 °C and, hence, is unlikely to modify the bulk lifetime under investigation. The Al₂O₃ films were removed with an HF(1%):HCl(1%) dip for 1 min, followed by a SC2 step for 10 min, a TMAH (25%) etch at 75–80 °C for 10 min, and then a second SC2 step for 10 min. Between each of these steps, samples were rinsed in de-ionized water. Finally, the samples were given a 1 min pre-treatment in HF(1%):HCl(1%) to terminate the surface with hydrogen¹⁹ followed by a treatment in TFSI-pentane (2 mg of TFSI per ml pentane) for 1 min. Samples were then re-characterized by PCD effective lifetime measurements and PL imaging in Warwick.

DLTS was performed on carefully selected regions from the two-sided Al₂O₃ passivated sample annealed at 400 °C which had been exposed to muons from one side only. Two adjacent samples ($\sim 4 \times 10 \text{ mm}^2$) were cleaved from the region of muon exposure, which was identified by PL imaging. DLTS was performed using diodes formed on the muon-exposed side in one sample, and the side not exposed to muons in another sample. DLTS sample preparation involved cleaning (trichloroethylene, acetone, and methanol), the formation of circular Schottky barrier diodes (2 mm diameter) by thermal evaporation of gold through a shadow mask, and the formation of an Ohmic contact by thermal evaporation of aluminum over the entire back surface. Samples were mounted on ceramic substrates with silver paint and the diodes were connected to contact pads with gold wire.

III. RESULTS

A. Photo- μ SR on wafer samples passivated on one side

We first present results of photo- μ SR effective lifetime experiments on a one-sided Al₂O₃ passivated silicon sample (sample A). The Al₂O₃ passivation scheme has been demonstrated to give a surface recombination velocity (SRV) of <1 cm/s in our laboratory,¹⁹ as confirmed by the PCD effective lifetime measurements on the double sided passivated sample exceeding 20 ms [Table I and Fig. 1(a)]. The unpassivated surface had an SRV several orders of magnitude higher and this limited the PCD effective lifetime to well below 1 ms in the one-sided passivated case.

The results of two sets of experiments for this sample are shown in Fig. 2. The first set of experiments used different degraders to control the implantation depth of the muon probe, with simulated muon distributions shown in Fig. 2(a). The lifetime spectra, which are plots of excess carrier density (Δn) obtained from the photo- μ SR technique vs the time difference between the laser and muon pulses (Δt), are shown in Fig. 2(b). As will become clear later, the chronological order in which the experiments were performed can be important, and the ordering in the legend reflects this. An indication of the effective lifetime from photo- μ SR (denoted as $\tau_{\text{exponential}}$) is given by fitting an exponential decay of the form

$$\Delta n = n_0 \exp\left(-\frac{\Delta t}{\tau_{\text{exponential}}}\right) \quad (1)$$

to the experimental data. The fits in Fig. 2(b) give $\tau_{\text{exponential}}$ as 193, 189, 178, and 158 μ s for the muon distributions with peaks at

depths of 521, 392, 269, and 166 μ m, respectively. It is noted that simple exponential approach results in a relatively poor agreement with the experimental data at low values of Δn , and this effect occurs because the lifetime is dependent on Δn itself, as discussed later. This trend of reduced effective lifetime closer to the unpassivated surface is consistent with a relatively high rate of recombination occurring there. For the nearest surface muon implantation (52 μ m deep peak), the muon lifetime spectrum cannot be fitted with a single exponential decay, and similar behavior has been observed previously.³ We measure Δn as a function of Δt , which is a convolution of all muons in the envelope plotted in the relevant distribution in Fig. 2(a). At $\Delta t = 0$ (i.e., when the muon and light pulses arrive simultaneously), the carrier density is almost uniform as a function of depth. As Δt increases, very fast carrier recombination occurs at the unpassivated surface (probably limited by the thermal velocity), and Δn decays more rapidly than at deeper muon implantation depths where the carrier dynamics are dependent mainly on carrier diffusion. We, therefore, choose not to compare the carrier dynamics in the near surface region with those in the bulk.

The second set of photo- μ SR experiments on the one-sided passivated sample aimed to assess the stability of the measurement and to demonstrate that consistent lifetime measurements can be made with muon implantation into either side of the sample. The sample was measured twice with the muon beam passing through the unpassivated surface. The sample was then flipped over and was measured twice with the same degrader configuration. The muon depth distributions are shown in Fig. 2(c), and it is noted that the muon peak is closer to the unpassivated surface when the muons enter the sample through the passivated side rather than the unpassivated one. The corresponding photo- μ SR lifetime spectra in Fig. 2(d) are similar for all four measurements. When fitted with single exponential decays, the latter two measurements with muons incident from the passivated side give marginally lower values of $\tau_{\text{exponential}}$ than those when muons are incident from the unpassivated side. This likely originates from the slight shift of the muon distribution closer to the unpassivated surface. There is no evidence of lifetime degradation upon repeat measurement.

B. Photo- μ SR on wafer samples passivated on both sides

We next present results for high-lifetime silicon wafer samples passivated on both sides. As in the one-sided case, a series of photo- μ SR experiments was first performed using muon implantations at different depths, with the simulated muon depth distributions shown in Fig. 3(a). The long lifetimes mean that the laser repetition frequency was set at 12.5 Hz (instead of the usual 25 Hz), as shown in the timing diagram in Fig. 3(b). Photo- μ SR data for two samples are shown in Figs. 3(c) and 3(d). Measurements were made in the order used in the legend and for each case we first discuss the initial measurement made with a peak muon depth of 392 μ m. Fits of the initial photo- μ SR measurements give $\tau_{\text{exponential}}$ as 5.4 and 7.1 ms for the two-sided passivated samples activated at 350 °C (sample B) and 400 °C (sample C), respectively, compared to 189 μ s for the one-sided case (activated at 450 °C, sample A). These values are broadly consistent with the PCD effective lifetime

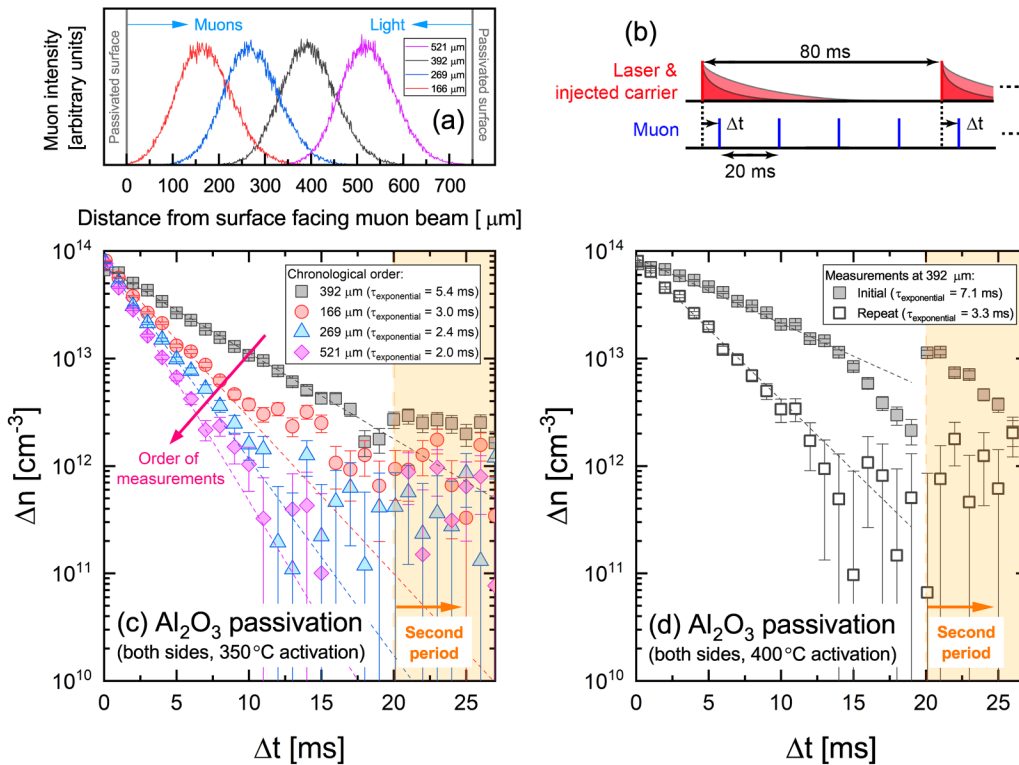


FIG. 3. Photo- μ SR data for silicon wafer samples (750 μ m thick) passivated with Al₂O₃ on both sides measured with the muon depth profiles shown in (a). (b) Timing diagram showing the laser running at 12.5 Hz, which was necessary for the long effective lifetimes in these samples. The diagram also shows carrier lifetime spectra (long and short) schematically illustrating how the carrier density is measured for timings Δt , $\Delta t + 20$ ms, $\Delta t + 40$ ms, and $\Delta t + 60$ ms. Data in (c) for sample B were acquired with different muon implantation depths with experiments performed in the order stated in the legend. Data in (d) for sample C were acquired at the same implantation depth. For these experiments, Δt was sequentially measured from 0 ms, where the sample was already degraded when $\Delta t = 19$ ms was measured. The long effective lifetimes mean photoexcited charge carriers remain when the second muon pulse arrives after 20 ms, which explains the artificial jump in excess carrier density after this Δt value, which is particularly apparent in the initial measurements in (d).

data in Fig. 1(a), noting the PCD data are dependent on excess carrier density. Differences will also arise because the PCD lifetime technique measures over whole thickness of the sample whereas photo- μ SR is more localized according to the muon distribution.

We note the apparent increase in excess carrier density at Δt of 20 ms, which is particularly clear in Fig. 3(d). This is a real signal which results from sample carrier lifetime degradation during the experiment and because of the way the data are acquired in the period mode which is described in Sec. II B. Note that the data point for $\Delta t = n$ ms (where n is an arbitrary delay) is acquired in the same run as for $\Delta t = n + [20, 40, 60]$ ms, where 20 ms is muon pulse separation [shown schematically in Fig. 3(b)]. Therefore, n only needs to scan $0 < n < 20$ ms to cover the entire time (i.e., $0 < \Delta t < 80$ ms). This causes an interesting effect when the carrier lifetime is degrading during the measurement cycle measuring from a low to high n . The level of carrier lifetime degradation is smallest for the data points for $n = 0$ ms, hence, at $\Delta t = 0, 20, 40$, and 60 ms. Carrier lifetime degradation increases progressively, and by the time $n = 19$ ms is measured, the measured excess carrier density is lower than it would be earlier in the cycle, and

this, therefore, leads to the step at $\Delta t = 20$ ms. Previous studies used samples with much shorter effective lifetimes and did not observe such an effect.^{1–3}

Uniform silicon samples passivated identically on both surfaces should have a symmetric effective lifetime depth profile, with a peak in the center and a decay toward both surfaces as the contribution from surface recombination (still significant even in well-passivated samples) becomes larger. Our intended aim was to use depth-dependent photo- μ SR to understand charge carrier recombination kinetics at a well-passivated surface, but during the beamtime session it became clear this would not be possible. In Fig. 3(c), the experiments were performed in the order shown in the legend, with the first muon implantation peak close to the center of the sample resulting in $\tau_{\text{exponential}}$ of 5.4 ms and the second muon implantation peak much closer to the surface giving a lower value of 3.0 ms. At this stage, the reduction in lifetime could be explained by increased proximity to the surface resulting in more surface recombination, yet a third measurement performed at a muon probe depth in between the first measurements gave a lower value still (2.4 ms). A fourth measurement—with the muons implanted

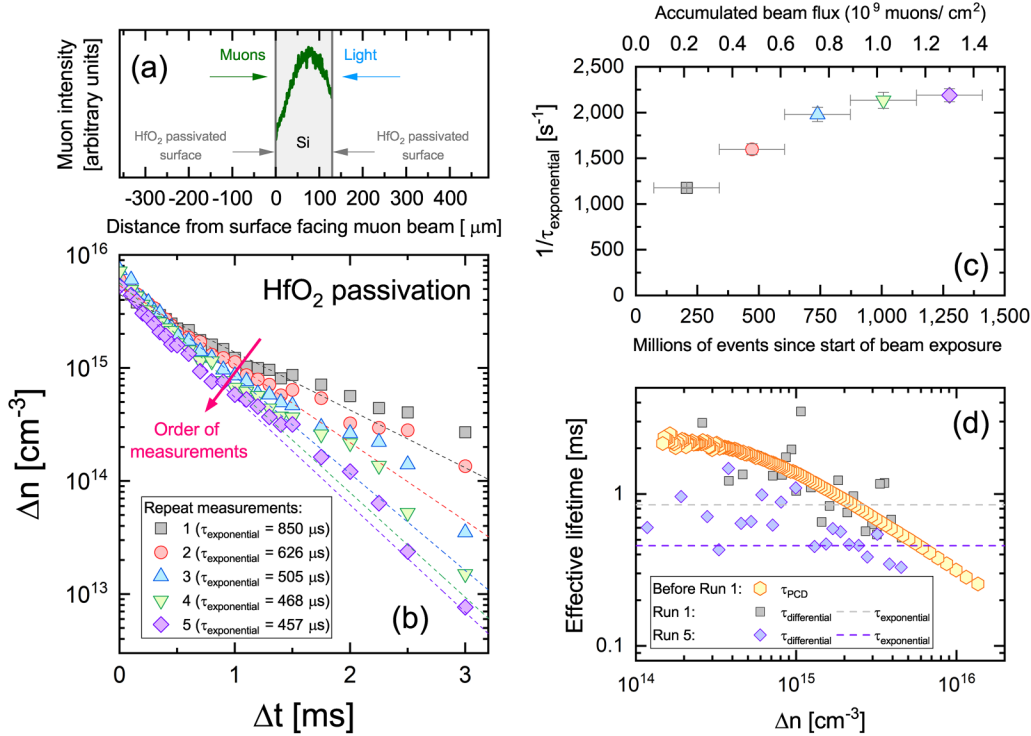


FIG. 4. Results from a series of repeat measurements on sample D, which is a HfO₂ passivated silicon sample (130 μm thick). The simulated muon depth profile is plotted in (a) on the same depth scales as Figs. 2(a) and 3(a). The photo- μ SR spectra in (b) are for five successive measurements (each 10 MeV per point), with experimental data fitted with the exponential effective lifetimes indicated. The plot in (c) shows the recombination rate which is $1/\tau_{\text{exponential}}$ from (b) vs, on the bottom axis, the number of aggregated events since the photo- μ SR experiment started with initial timing and power scans included (73.6 MeV), and on the top axis, vs the accumulated muon beam flux. Plot (d) shows a comparison of different effective lifetimes. Two of these are a function of excess carrier density: transient PCD before muon measurement, and photo- μ SR when analyzed in differential form [Eq. (2)]. Exponential photo- μ SR lifetimes that do not take into account the excess carrier density dependence [Eq. (1)] are also shown. Photo- μ SR lifetimes are shown for run 1 and run 5 to show that degradation has occurred.

to the far side of center—gave an even lower value (2.0 ms). It was, therefore, clear that the lifetime was not solely dependent on the muon implantation depth relative to the surface and that the lifetime was reducing as a consequence of the measurement. This finding was confirmed by measurements on a different two-sided passivated sample (sample C, 400 °C activation) with the measurement repeated at the same muon implantation depth close to the center of the sample. The data, shown in Fig. 3(d), show a lifetime reduction from 7.1 to 3.3 ms at the same location, which is clear evidence for the lifetime degrading during the measurement.

A systematic degradation study was performed on the silicon sample with HfO₂ passivation on both sides (sample D), with results from five experimental runs presented in Fig. 4 (each data point counted for 10 MeV). This sample was just 130 μm thick and the simulated muon depth profile is shown in Fig. 4(a). The photo- μ SR results in Fig. 4(b) show the excess carrier density at a given Δt reduces with each measurement run, with values of $\tau_{\text{exponential}}$ shown in the legend. Figure 4(c) shows the recombination rate ($1/\tau_{\text{exponential}}$) increases with the number of detector events (bottom axis). The top axis of Fig. 4(c) shows the accumulated beam flux which was calculated by multiplying the detector counts

by a geometric factor to take into account the solid angle coverage of positron detectors in HiFi (25%) and dividing by the estimated muon beam area of 3.925 cm². The recombination rate is sublinear with beam exposure, which means that is likely the density of recombination centers is not directly proportional to the accumulated beam flux. Linking a recombination rate (or carrier lifetime) to a defect concentration is not possible without knowledge of the capture cross sections of the defect. Furthermore, DLTS results shown later demonstrate the formation of multiple recombination-active defects as a consequence of the muon exposure, with each defect potentially having a different concentration and capture cross section.

A limitation of using $\tau_{\text{exponential}}$ as a measure of effective lifetime arising from photo- μ SR experiments is that its calculation from the Δn vs Δt plot assumes the effective lifetime is independent of Δn itself. This explains the relatively poor fits of photo- μ SR data with a simple exponential function in Figs. 2–4. In reality, semiconductor carrier recombination processes however—whether intrinsic (e.g., radiative, Auger) or extrinsic (e.g., Shockley-Read-Hall, SRH)—depend on excess carrier density. To take into account the dependence on excess carrier density, we can calculate a

differential effective lifetime, $\tau_{\text{differential}}$, from photo- μ SR lifetime data according to

$$\tau_{\text{differential}} = -\frac{\Delta n_{\text{average}}}{\left(\frac{\Delta(\Delta n)}{\Delta(\Delta t)}\right)}, \quad (2)$$

where $\Delta n_{\text{average}}$ is the mean of two adjacent measured Δn values, $\Delta(\Delta n)$ is the difference between two adjacent Δn values, and $\Delta(\Delta t)$ is the difference between the two adjacent corresponding Δt values. This approach is flawed due to the integrative nature of the Δn values determined from the spin depolarization rate (λ) over the measured time window but Eq. (2) can be used to determine $\tau_{\text{differential}}$ at different values of $\Delta n_{\text{average}}$ that are more compatible with the results of conventional effective lifetime measurements via PCD or modulated PL than $\tau_{\text{exponential}}$.

We apply Eq. (2) to the photo- μ SR data recorded on the HfO_2 passivated sample. The resulting $\tau_{\text{differential}}$ curves from the first and fifth photo- μ SR measurements are shown in Fig. 4(d) alongside the curve measured via PCD pre-muon exposure already shown in Fig. 1(a). The Δn value for photo- μ SR is taken as $\Delta n_{\text{average}}$, and we have first averaged $\Delta(\Delta n)$ over two adjacent points to reduce noise. The initial effective differential lifetime from photo- μ SR is consistent with PCD effective lifetime, although the photo- μ SR data are significantly noisier even after two-point averaging. The degradation between the first and fifth runs is clearly evident in the $\tau_{\text{differential}}$

data. The effective lifetimes from photo- μ SR are dependent on excess carrier density, and this shows the limitation of using a simple $\tau_{\text{exponential}}$ approach. The corresponding values of $\tau_{\text{exponential}}$ from the fits in Fig. 4(b) are shown in Fig. 4(d) as horizontal dashed lines, and these lie within the range of values taken by $\tau_{\text{differential}}$ for different values of excess carrier density. Further optimization of the measurement routine is needed for the extraction of excess carrier lifetime from photo- μ SR data. Results presented in Fig. 4 demonstrate that the photo- μ SR technique can be applied to silicon wafers of the thickness typically now used for silicon photovoltaic cells.

C. Understanding the lifetime degradation

Wafer samples have been shown to degrade after exposure to the muon beam. The reduction in effective lifetime in high-lifetime silicon (Figs. 3 and 4) could be due to increased surface recombination as a consequence of damage to the passivation layer (either Al_2O_3 or HfO_2), the formation of recombination centers in the bulk, or a combination of both. Additional experiments were performed on the samples after the photo- μ SR experiments to understand the degradation which had occurred.

All samples from the photo- μ SR experiments were first characterized by PL imaging. A circular region of low PL signal coinciding with the location of the muon beam was detected, with an example shown for Al_2O_3 passivation (sample C) in Figs. 5 and 6. The size of the low PL region is smaller than the

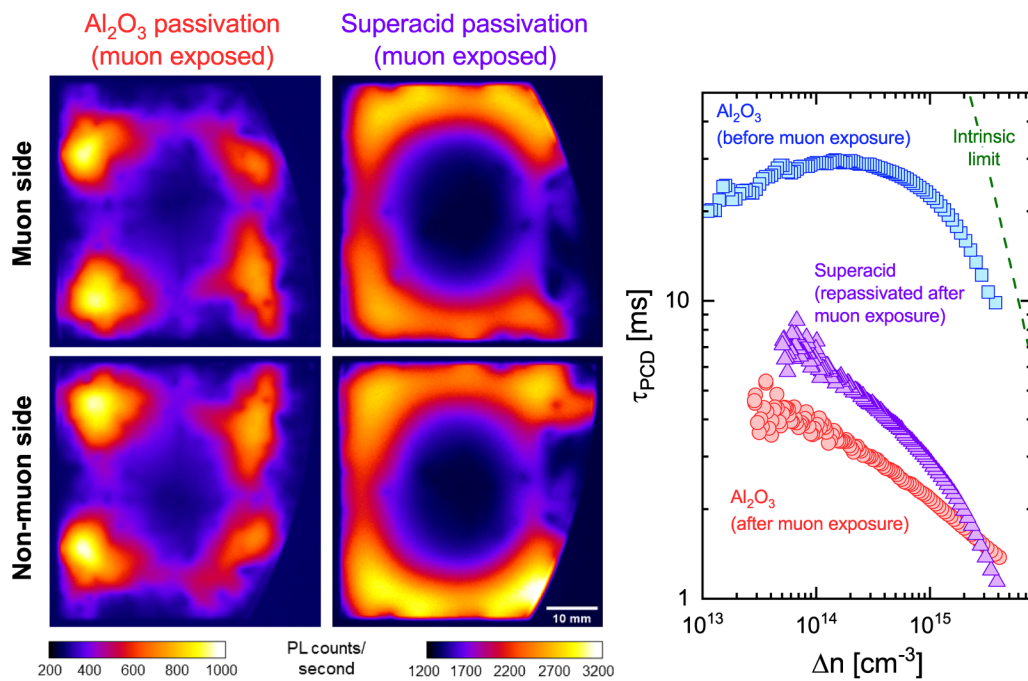


FIG. 5. Results of a re-passivation experiment on sample C whose corresponding photo- μ SR data are shown in Fig. 3(d). The left-hand PL images (0.758 W/cm^2 , 5 s exposure) are with Al_2O_3 passivation; the right-hand PL images (0.758 W/cm^2 , 1 s exposure) are with superacid-based passivation using the University of Warwick PL system. Both images were taken after the sample had been exposed to muons. The PCD effective lifetime curves are from the same sample with Al_2O_3 passivation before muon exposure, Al_2O_3 passivation after muon exposure, and with superacid passivation after muon exposure. The intrinsic lifetime limit of Niewelt *et al.*²⁰ is also plotted.

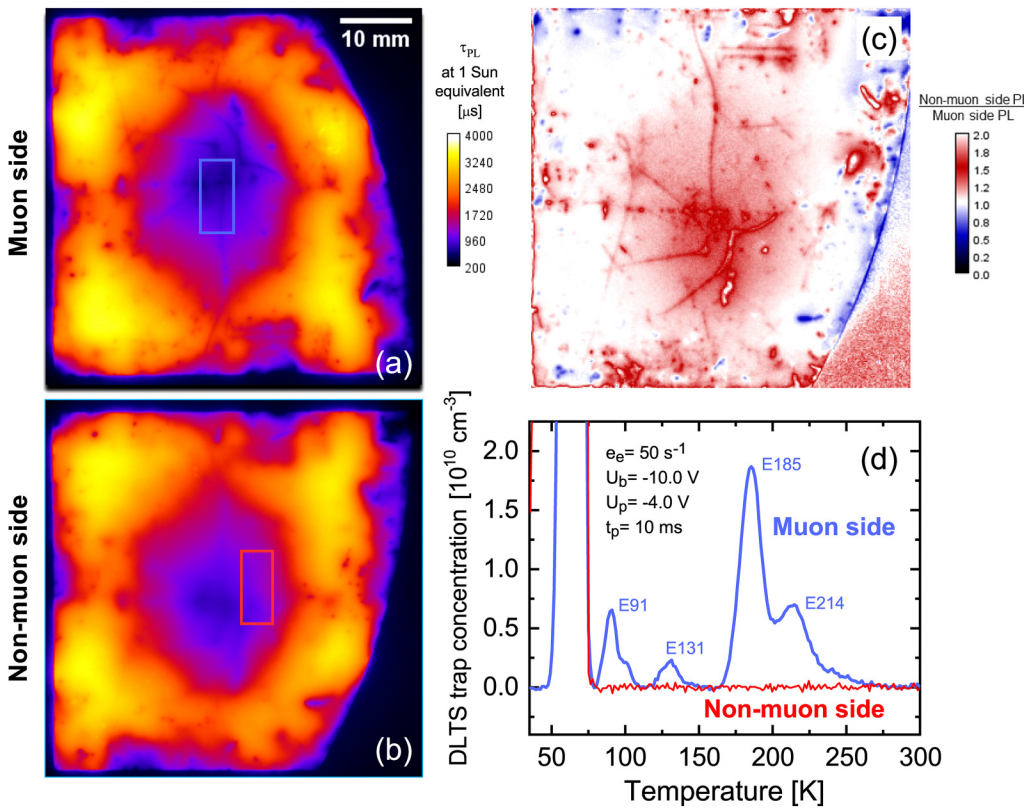


FIG. 6. Post-muon exposure characterization results from sample C whose corresponding photo- μ SR data are shown in Fig. 3(d). Calibrated PL effective lifetime images (1 Sun illumination for 5 s) from the Fraunhofer ISE system with a common scale bar from (a) the muon exposed side and (b) the side of the sample which was not muon exposed. The ratio of lifetimes at equivalent locations from the non-muon exposed side to the muon exposed side is plotted in (c), so values >1 indicate higher PL signal from the non-muon side. DLTS trap concentrations defined as Y in Eq. (3) are shown in (d) for samples extracted from the approximate locations of the rectangles shown in (a) and (b). Measurement settings shown on the graph are the rate window (e_e), bias voltage (U_b), filling pulse voltage (U_p), and filling pulse length (t_p).

3 cm diameter optical excitation aperture shown in Fig. 1(d), so hence we discount the possibility of light-induced degradation of the surface passivation or bulk lifetime. The degraded region in PL extends beyond the size of the muon beam profile (approximately 12 mm circular), and, in the calibrated PL images in Figs. 6(a) and 6(b), the lifetime level can be seen to increase radially from the location of the beam center. As high purity low or moderately doped silicon has a very long carrier diffusion length, the effects of a high recombination region or surface will extend beyond that region, as carriers from low recombination regions diffuse to and recombine in the high recombination region or surface (i.e., carrier diffusion smearing).

We next consider the possibility that the muon beam might only degrade the passivating dielectric layer, which, if true, would make the passivation level not uniform across the sample and could result in a non-uniform PL image. We have performed an experiment to re-passivate a muon-exposed sample, with the results presented in Fig. 5 for sample C, which was passivated on both sides with Al_2O_3 and exposed to muons from one side. The Al_2O_3 passivation was chemically removed and the sample was

etched before being re-passivated with a superacid-based scheme. The uncalibrated PL images after re-passivation show higher PL count rates (due to better passivation), yet the central dark region remains. This proves that the lifetime degradation during photo- μ SR cannot be explained by surface passivation degradation alone and so the bulk lifetime must have degraded. The etching prior to superacid re-passivation removes $\sim 5 \mu\text{m}$ from each surface, which implies any beam damage is deeper than this.

Effective lifetime curves measured by PCD are shown in Fig. 5 for the same sample with Al_2O_3 passivation prior to muon exposure, after muon exposure, and after subsequent replacement of the Al_2O_3 with superacid-based passivation. Prior to muon exposure, the effective lifetime was high, approaching the intrinsic limit of Niewelt *et al.* at high excess carrier densities,²⁰ taking a value of 22.6 ms at 10^{15} cm^{-3} . Muon exposure reduced the effective lifetime at the same excess carrier density to 2.2 ms with Al_2O_3 passivation and 2.9 ms after superacid re-passivation. The PL images show that the lifetime distribution after muon exposure is not uniform over the measurement area of the photoconductance coil (2 cm diameter in the setup used). The measured effective lifetime curves will,

therefore, be affected by contributions from outside the muon exposed region and hence will overestimate the actual effective lifetime in the exposed region. Nonetheless, the results confirm that degradation has occurred in the bulk as a consequence of the muon exposure. The slight increase in effective lifetime after superacid re-passivation may be indicative of additional muon beam damage occurring to Al_2O_3 , as the surface recombination velocity of the superacid scheme at 1 cm/s or slightly less^{16,17,21} is similar to what we would expect with our Al_2O_3 passivation scheme. It is also possible that passivation degradation occurs during sample handling for the beamline experiments, and the superacid-passivation acts to recover passivation lost because of small near-surface scratches. It is, however, proven that passivation degradation alone cannot explain the degradation observed.

Further evidence of beam-related damage can be gained by characterizing sample C from Figs. 5 and 6 from alternate sides, as differences are to be expected as muons were only implanted through one surface of this sample. Qualitatively, PL images show lower lifetime regions at the muon beam location when measured from either side because even on the remaining lifetime level carriers generated near the non-muon exposed surface can easily reach the muon exposed region in which they can more rapidly recombine. However, due to the exponential drop of light absorption and application of a 1050 nm shortpass filter in the PL imaging system, an intensity difference can be expected if recombination occurs closer to or at one surface.²² Figure 6(c) shows the ratio (at the equivalent position) of the PL intensity measured from the non-muon exposed side to that from the muon exposed side. Away from the central region and not near the sample edges, the ratio is approximately unity (white) apart from surface scratches and passivation flaws such as the wrap-around at the sample edges. In the muon-exposed central region, the ratio is greater than 1 (red), which means there is less recombination close to the non-muon exposed surface. A full quantitative analysis from PL imaging is beyond the scope of this work because accounting for the unknown depth distribution of the damage would require extensive additional characterization.

Lifetime techniques are extremely sensitive to defect-related recombination in silicon, but using them to identify defects is usually only possible when the sample set is deliberately well controlled,²³ which is not the case here. We, therefore, applied DLTS to provide further insight into the recombination active defects and test the hypothesis of them being more prevalent close to the muon exposed surface. DLTS samples were extracted at the locations indicated by the rectangles in the PL images in Figs. 6(a) and 6(b). DLTS is sensitive to electrically active states relatively close to the surfaces. Figure 6(d) shows the DLTS spectra recorded with a rate window of 50 s⁻¹ for Schottky diodes made on both sides of the photo- μ SR sample, including the one which was not muon exposed. Concentration values are plotted in Fig. 6(d) and these are defined as

$$Y = 2 \frac{\Delta C}{C_b} N_d f, \quad (3)$$

where ΔC is the magnitude of a capacitance transient, C_b is the bias capacitance, N_d is the concentration of ionized dopant atoms,

and f is the correction function, which takes into account depletion widths at the bias and pulse voltages.²⁴ The so-defined Y values at the peak maxima are close to the corresponding trap concentrations.

A large emission signal with its peak maximum at 66 K is observed in both spectra, and this is likely to arise from a substrate-related trap and not from the muon experiment. We attribute this peak to the second donor level of oxygen-related thermal double donors.^{25,26} Oxygen-related defects are expected in Czochralski-grown silicon, which usually has an interstitial oxygen concentration of order 10^{17} – 10^{18} cm⁻³.^{27,28} The high resistivity of this sample ($2000 \Omega \text{ cm}$) suggests that a magnetic field was used to control convection in the melt and this usually gives an oxygen concentration closer to 10^{17} than to 10^{18} cm⁻³.²⁹ Oxygen-related double donor defects are formed during crystal cooling or even at the temperatures used for passivation activation.^{28,30}

The key finding from DLTS is the difference between the muon exposed and non-muon exposed sides at higher temperatures in Fig. 6(c). Four electron traps are found to exist in the muon implanted side, which are absent in the other side. These are labeled as E91, E131, E185, and E214, where "E" means electron trap and the number is temperature of the corresponding peak maximum. The concentrations of the traps are of order 10^{10} cm⁻³ as can be seen from the DLTS spectrum in Fig. 6(d). Defect concentrations of this order of magnitude are consistent with the level of effective lifetime degradation observed.

D. Lifetime measurements in completed PERC solar cells

Finally, we turn our attention to effective lifetime measurements in completed gallium doped silicon PERC solar cells, which have a similar thickness to the HfO_2 passivated sample studied previously. Effective lifetimes for cells are more challenging to interpret than those in wafer samples, for which the effective lifetime usually only has contributions from the bulk lifetime and surface recombination. Cells also feature diffused regions and laterally distributed metal contacts, so the effective lifetime in cells tends to be much lower than in wafer-level samples and the results are much more complex to interpret.

Calibrated PL effective lifetime images of the cells after the photo- μ SR experiments using the harmonically modulated technique at Fraunhofer ISE are shown in Fig. 7(a). The PL originating from underneath the metal contacts does not reach the camera due to shading. Such features are, therefore, dark, as are the corner regions of the $0.6 \Omega \text{ cm}$ cell where mounting tape from the photo- μ SR experiments remained. Photo- μ SR lifetime spectra from all three cells are shown in Fig. 7(b). The curves are in order of the cell substrate resistivity, with Δn being relatively higher for increasing levels of substrate resistivity. The fits of $\tau_{\text{exponential}}$ shown give values of $25.6 \mu\text{s}$ for $1 \Omega \text{ cm}$, $20.7 \mu\text{s}$ for $0.6 \Omega \text{ cm}$, and $12.7 \mu\text{s}$ for $0.3 \Omega \text{ cm}$, although it is noted that the extent to which the experimental data can be fitted with a simple exponential is questionable. Figure 7(c) shows effective lifetimes from the harmonically modulated technique, τ_{PL} , vs excess carrier concentration, with the lifetimes also increasing in the same order of substrate resistivity.

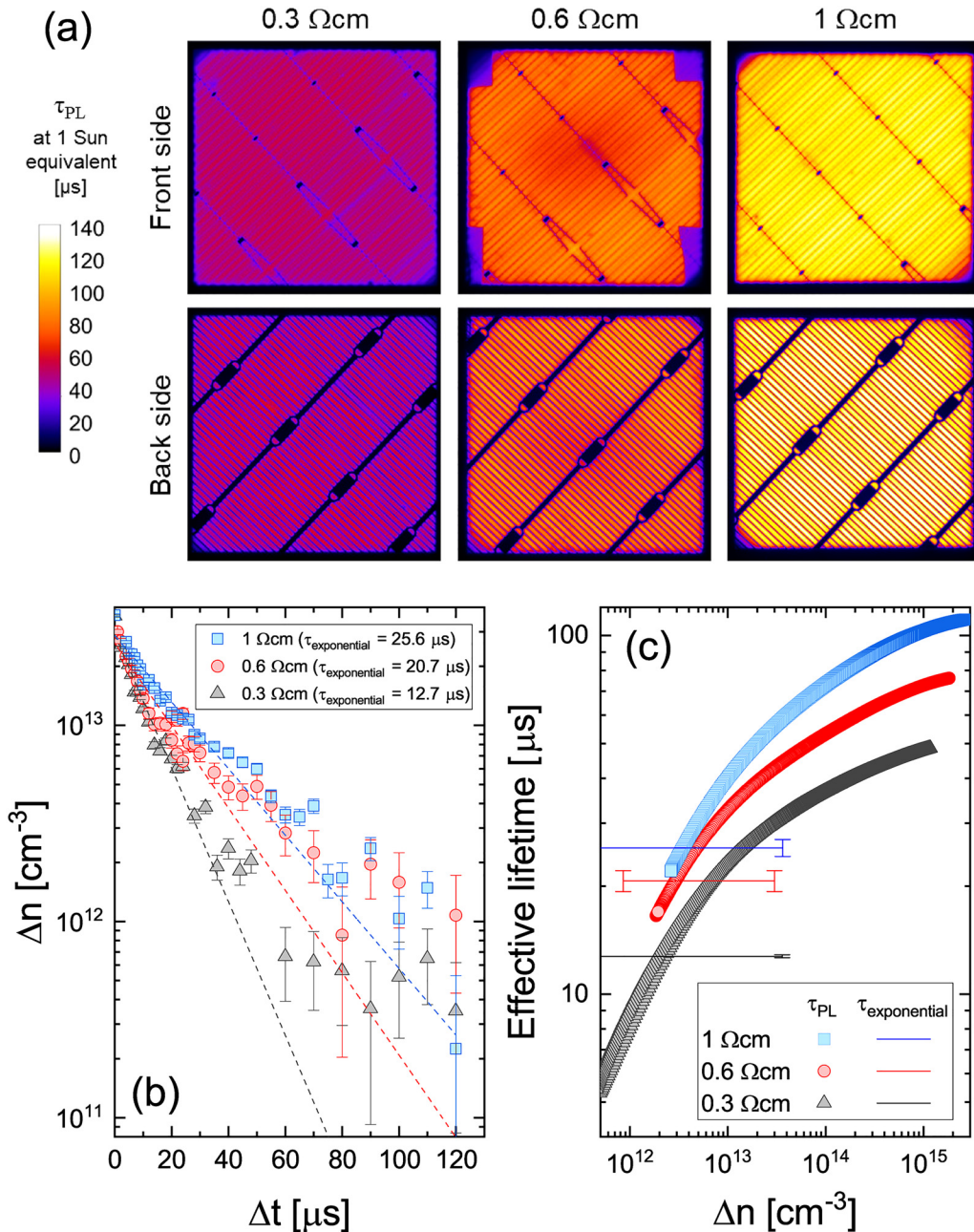


FIG. 7. Results for gallium doped silicon PERC solar cells ($150\ \mu\text{m}$ thick). (a) Calibrated PL lifetime images for $5 \times 5\ \text{cm}^2$ samples acquired under 1 Sun equivalent conditions after photo- μ SR experiments. (b) Spectra from photo- μ SR experiments measured with muons implanted into the back side of the samples shown in (a), with fits according to the exponential effective lifetimes stated. (c) Effective lifetimes as a function of excess carrier density measured on the cells in (a) from harmonically modulated luminescence measurements. The exponential effective lifetimes from the fits to the photo- μ SR data in (b) are overlaid on the plot in (c) with the excess carrier density range indicated.

The $\tau_{exponential}$ values from Fig. 7(b) are consistent with the harmonically modulated PL data in Fig. 7(c), and the strong variation with excess carrier density in the latter explains the relatively poor fit of Eq. (1) to the photo- μ SR data.

Figure 7(a) shows that the measured effective lifetime by PL under 1 Sun equivalent conditions in the $0.3\ \Omega\text{ cm}$ and $1\ \Omega\text{ cm}$ cells is uniform; however, there is circular region of slightly lower lifetime in the $0.6\ \Omega\text{ cm}$ cell. This degraded region coincides with the

location of the muon beam. The detection of muon beam-related degradation in the $0.6\ \Omega\text{ cm}$ cell and not the others is likely due to the $0.6\ \Omega\text{ cm}$ cell being exposed to the muon beam for considerably longer (34.8 h total, compared to 5.5 h for $0.3\ \Omega\text{ cm}$ and 7.3 h for $1\ \Omega\text{ cm}$, as shown in Table II). This cell was also measured from both sides, whereas the others were only measured from the rear.

IV. DISCUSSION

A. Lifetime in thin wafers and completed solar cell devices

We have shown it is possible to use photo- μ SR to measure effective lifetimes in thin wafers ($130\ \mu\text{m}$ thick) with the results consistent with PCD measurements (Fig. 4). We have also shown that photo- μ SR can be used to measure effective lifetimes in completed PERC solar cells, with the results being consistent with harmonically modulated PL imaging (Fig. 7). As expected, the measured effective lifetimes of our gallium doped PERC samples scale with their resistivity and lifetimes in solar cells are shorter than in passivated wafers. A recent study has shown the carrier lifetime in gallium doped silicon wafers varies strongly with resistivity.³¹ At $\Delta n = 3 \times 10^{13}\ \text{cm}^{-3}$, the PCD effective lifetime is approximately $50\ \mu\text{s}$ for a $0.3\ \Omega\text{ cm}$ wafer and approximately $180\ \mu\text{s}$ for a $1\ \Omega\text{ cm}$ wafer.³¹ The effective lifetimes in the completed cells we measured either by photo- μ SR or harmonically modulated PL at a similar excess carrier density are lower than this. This is to be expected as the effective lifetime in cells is reduced by recombination in the highly doped emitter region and because of additional recombination in the vicinity of the contacts.

We note differences in the dependence of effective lifetime on excess carrier density between wafer and cell samples. For wafer samples, the impact of intrinsic (Auger and radiative) recombination²⁰ becomes apparent at higher excess carrier densities in both PCD and photo- μ SR data [see Fig. 4(d) for a direct comparison for sample D]. For lower excess carrier densities, the behavior in the high-lifetime moderately doped wafer samples is consistent with there being little recombination activity associated with bulk defects. This is evidenced by the lifetime curve for sample C in Fig. 1(a). Of the two-sided passivated samples, the activation conditions for sample C were closest to optimal, and there is not a dependence of effective lifetime on excess carrier density which would likely occur if there were high levels of defect-related SRH recombination. The effective lifetime at low excess carrier densities in wafer samples is probably limited by residual surface recombination even after surface passivation. The PERC solar cell lifetimes in Fig. 7, on the other hand, are likely limited by additional recombination sources, including bulk defect limitations due to process contamination and recombination due to the diffused emitter—which also implies strong lateral conduction toward localized recombination center such as the metal-Si contacts or sample edges. These recombination types and their superposition often create an increasing effective lifetime with rising carrier density, as shown in previously harmonically modulated PL studies of solar cells.^{8,9}

B. Muon beam damage

Generally, muons are considered to be passive probes, which do not disturb their surroundings.³² The case presented here,

however, suggests that beam damage by muons can significantly reduce bulk carrier lifetime, although this effect is observable only in high-lifetime silicon wafers. In samples with lower effective lifetimes, muon-induced recombination activity will still occur, yet its effect will not be as apparent due to the simultaneous existence of stronger recombination channels, such as the unpassivated surface in the case of sample A. The concentration of defects created by the beam is not high, but it can be sufficient to affect high lifetimes in extremely pure samples that are well passivated. Evidence gained for muons affecting the sample as a consequence of photo- μ SR measurements includes (i) the location of low lifetime region in PL matching the position of the muon beam; (ii) the size of the low lifetime region in PL being consistent with the muon beam size (and not the area of optical excitation); (iii) the systematic decay in effective lifetime during the muon experiment [Fig. 4(b)]; and (iv) the existence of electrically active states in DLTS in the muon exposed side of the sample and not in the other [Fig. 6(d)]. The concentration of electrically active states formed (of order $10^{10}\ \text{cm}^{-3}$) is sufficient to degrade the effective lifetime of high lifetime silicon wafers when they are well passivated.

We have achieved a relatively low effective lifetime by passivating the wafer on just one side with Al_2O_3 , similar to the relatively poorly passivated wafer with a hydrogen terminated surface used in Ref. 3. Our study confirmed that it is possible to measure depth-dependent carrier lifetimes with photo- μ SR as the effective lifetime is too low to detect recombination arising from the beam damage. For longer effective lifetimes, substantial degradation occurs during the measurement and the measurement history of the sample needs to be accounted for in the interpretation of results.

We are not aware of prior reports of muon-induced defect formation specifically, although implantation of MeV electrons, protons, γ -rays, and various ions have been found to induce electrically active defects in silicon.^{33–36} For example, studies of *n*-type silicon irradiated by 1.3 MeV protons can give rise to DLTS spectra with five electron traps,³³ which are not dissimilar to the data in Fig. 6(c) for which the muon energy at the silicon surface is approximately 2.8 MeV. The muon implantations were not carried out in a sufficiently controlled way for us to be able to assign DLTS peaks to specific crystallographic defects. Future work will focus on producing sample sets with sufficient control for detailed specific studies. Experiments should also be performed to determine whether muon-related degradation can be recovered, either by thermal annealing or by bulk passivation.

C. Advantages and disadvantages of the photo- μ SR lifetime technique

Photo- μ SR has two main advantageous features over conventional lifetime techniques such as PCD or standard PL imaging. The first is that lifetime information can relatively easily be acquired as a function of depth into a bulk material by lowering the muon beam energy with the insertion of degrader material in the beam path. The second is that effective lifetimes can be measured in completed devices, such as solar cells, by virtue of the penetrating nature of muon beams. The photo- μ SR lifetime technique can be applied to semiconductors other than silicon, although it is noted that relatively wide distribution of the muon probe at ISIS

($\text{FHWM} > 100 \mu\text{m}$) means these have to be bulk samples as opposed to thin films. The technique has been applied to germanium previously,² but measurement should be possible in principle for other bulk indirect gap semiconductors (e.g., SiC, diamond).

Photo- μ SR should not be seen as a direct replacement for lifetime measurement problems in which more conventional lifetime measurement approaches are suitable. Access to a suitable muon beamline is required and the measurement times are relatively long (each lifetime curve for a given degrader configuration takes several hours to acquire). We have shown in this paper that the muon beam degrades the material under investigation. This poses a measurement challenge for the highest quality silicon materials where defect-mediated SRH recombination is minimal in the starting material. Other indirect gap bulk semiconductors typically have much higher levels of grown-in SRH recombination than silicon due to impurity- and defect-related states, and the level of additional SRH recombination introduced by the muon beam may well be negligible in such cases. We, therefore, conclude that photo- μ SR can be a valuable technique for measurement of depth-dependent lifetime and in completed devices, provided any degradation during the measurement is negligible or fully taken into account.

V. CONCLUSIONS

Photo- μ SR has been used to measure effective lifetimes in silicon, with the results consistent with those from PCD methods for wafer samples with thicknesses down to $130 \mu\text{m}$ and from harmonically modulated PL imaging in the case of solar cells. When a high-lifetime sample is passivated on just one side with high quality Al_2O_3 , it is shown that the effective lifetime varies systematically with muon implantation depth. When such a sample is passivated on both sides, recombination in the damaged region created by the muon beam reduces the effective lifetime being measured. We have also shown that photo- μ SR can be applied to completed solar cells, with effective lifetimes consistent with those from harmonically modulated PL imaging. Prolonged exposure of cells to the muon beam has also been shown to degrade the sample under investigation. A series of experiments has been performed to understand the degradation processes. By removing the Al_2O_3 passivation from the muon exposed samples and re-passivating them with a temporary superacid-based technique, we have proven that the lifetime of the silicon bulk has degraded. A comparison of calibrated PL images from the muon-exposed side to the side not exposed to muons shows that the lifetime is lower when closer to the surface exposed to muons. DLTS is used to demonstrate the existence of electrically active recombination centers in the muon exposed region. It is, therefore, clear that muons are not inert probes in photo- μ SR experiments, and their interaction with the sample should be considered in the interpretation of data.

ACKNOWLEDGMENTS

We acknowledge muon beam time at the STFC ISIS Facility as part of the experiment (No. RB2010023). The work was supported in part by a Leverhulme Trust Research Project Grant (No. RPG-2020-377). S.L.P. and A.W. were supported by EPSRC Doctoral Training Partnership studentships (No. EP/R513374/1).

The collaboration between Warwick and Fraunhofer ISE was supported by the EPSRC Supergen Solar Network+ (No. EP/S000763/1). The work in Manchester was funded by EPSRC (No. EP/T025131/1).

AUTHOR DECLARATIONS

Conflict of Interest

The authors have no conflicts to disclose.

Author Contributions

J. D. Murphy: Conceptualization (lead); Formal analysis (equal); Funding acquisition (lead); Investigation (equal); Methodology (equal); Project administration (lead); Resources (lead); Supervision (lead); Writing – original draft (lead); Writing – review and editing (lead). **N. E. Grant:** Conceptualization (supporting); Investigation (equal); Methodology (supporting); Writing – review and editing (supporting). **S. L. Pain:** Investigation (supporting); Methodology (supporting); Writing – review and editing (supporting). **T. Niewelt:** Formal analysis (equal); Investigation (equal); Methodology (supporting); Writing – review and editing (equal). **A. Wratten:** Investigation (supporting). **E. Khorani:** Investigation (supporting); Methodology (supporting). **V. P. Markevich:** Formal analysis (supporting); Investigation (equal); Methodology (supporting); Writing – review and editing (supporting). **A. R. Peaker:** Methodology (supporting); Supervision (supporting). **P. P. Altermatt:** Resources (supporting). **J. S. Lord:** Conceptualization (supporting); Formal analysis (supporting); Investigation (supporting); Methodology (supporting); Software (supporting); Writing – review and editing (supporting). **K. Yokoyama:** Conceptualization (equal); Formal analysis (equal); Investigation (equal); Methodology (equal); Software (equal); Writing – review and editing (equal).

DATA AVAILABILITY

The raw data underpinning this study are openly available from the ISIS Neutron and Muon Source Data Catalogue Ref. 37. The data that support the findings of this study are available from the corresponding author upon reasonable request.

REFERENCES

- ¹K. Yokoyama, J. S. Lord, J. Miao, P. Murahari, and A. J. Drew, “Photoexcited muon spin spectroscopy: A new method for measuring excess carrier lifetime in bulk silicon,” *Phys. Rev. Lett.* **119**, 226601 (2017).
- ²K. Yokoyama, J. S. Lord, P. W. Mengyan, M. R. Goeks, and R. L. Lichti, “Muon probes of temperature-dependent charge carrier kinetics in semiconductors,” *Appl. Phys. Lett.* **115**, 112101 (2019).
- ³K. Yokoyama, J. S. Lord, J. Miao, P. Murahari, and A. J. Drew, “Decoupling bulk and surface recombination properties in silicon by depth-dependent carrier lifetime measurements,” *Appl. Phys. Lett.* **118**, 252105 (2021).
- ⁴R. S. Bonilla, B. Hoex, P. Hamer, and P. R. Wilshaw, “Dielectric surface passivation for silicon solar cells: A review,” *Phys. Status Solidi A* **214**, 1700293 (2017).
- ⁵H. B. Profijt, S. E. Potts, M. C. M. van de Sanden, and W. M. M. Kessels, “Plasma-assisted atomic layer deposition: Basics, opportunities, and challenges,” *J. Vac. Sci. Technol. A* **29**, 050801 (2011).

- ⁶G. Dingemans and W. M. M. Kessels, "Status and prospects of Al₂O₃-based surface passivation schemes for silicon solar cells," *J. Vac. Sci. Technol. A* **30**, 040802 (2012).
- ⁷X. Cheng, P. Repo, H. Halvard, A. P. Perros, E. S. Marstein, M. Di Sabatino, and H. Savin, "Surface passivation properties of HfO₂ thin film on n-type crystalline Si," *IEEE J. Photovolt.* **7**, 479–485 (2017).
- ⁸J. A. Giesecke, B. Michl, F. Schindler, M. C. Schubert, and W. Warta, "Minority carrier lifetime of silicon solar cells from quasi-steady-state photoluminescence," *Sol. Energy Mater. Sol. Cells* **95**, 1979–1982 (2011).
- ⁹H. Höffler, F. Schindler, A. Brand, D. Herrmann, R. Eberle, R. Post, A. Kessel, J. Greulich, and M. C. Schubert, "Review and recent development in combining photoluminescence- and electroluminescence-imaging with carrier lifetime measurements via modulated photoluminescence at variable temperatures," in *37th European Photovoltaic Solar Energy Conference* (EU PVSEC, 2020).
- ¹⁰R. Preu, E. Lohmüller, S. Lohmüller, P. Saint-Cast, and J. M. Greulich, "Passivated emitter and rear cell—Devices, technology, and modeling," *Appl. Phys. Rev.* **7**, 041315 (2020).
- ¹¹P. P. Altermatt, Y. Chen, Y. Yang, and Z. Feng, "Riding the workhorse of the industry: PERC," *Photovolt. Int.* **41**, 46–54 (2018).
- ¹²K. Yokoyama, J. S. Lord, P. Murahari, K. Wang, D. J. Dunstan, S. P. Waller, D. J. McPhail, A. D. Hillier, J. Henson, M. R. Harper, P. Heathcote, and A. J. Drew, "The new high field photoexcitation muon spectrometer at the ISIS pulsed neutron and muon source," *Rev. Sci. Instrum.* **87**, 125111 (2016).
- ¹³J. S. Lord, I. McKenzie, P. J. Baker, S. J. Blundell, S. P. Cottrell, S. R. Giblin, J. Good, A. D. Hillier, B. H. Holsman, P. J. C. King, T. Lancaster, R. Mitchell, J. B. Nightingale, M. Owczarkowski, S. Poli, F. L. Pratt, N. J. Rhodes, R. Scheuermann, and Z. Salman, "Design and commissioning of a high magnetic field muon spin relaxation spectrometer at the ISIS pulsed neutron and muon source," *Rev. Sci. Instrum.* **82**, 073904 (2011).
- ¹⁴K. Sedlak, R. Scheuermann, T. Shiroka, A. Stoykov, A. R. Raselli, and A. Amato, "MusrSim and MusrSimAna - Simulation tools for μ SR instruments," *Phys. Procedia* **30**, 61–64 (2012).
- ¹⁵S. R. Giblin, S. P. Cottrell, P. J. C. King, S. Tomlinson, S. J. S. Jago, L. J. Randall, M. J. Roberts, J. Norris, S. Howarth, Q. B. Mutamba, N. J. Rhodes, and F. A. Akeroyd, "Optimising a muon spectrometer for measurements at the ISIS pulsed muon source," *Nucl. Instrum. Methods Phys. Res., Sect. A* **751**, 70–78 (2014).
- ¹⁶N. E. Grant, T. Niewelt, N. R. Wilson, E. C. Wheeler-Jones, J. Bullock, M. Al-Amin, M. C. Schubert, A. C. van Veen, A. Javey, and J. D. Murphy, "Superacid-treated silicon surfaces: Extending the limit of carrier lifetime for photovoltaic applications," *IEEE J. Photovolt.* **7**, 1574–1583 (2017).
- ¹⁷A. I. Pointon, N. E. Grant, E. C. Wheeler-Jones, P. P. Altermatt, and J. D. Murphy, "Superacid-derived surface passivation for measurement of ultra-long lifetimes in silicon photovoltaic materials," *Sol. Energy Mater. Sol. Cells* **183**, 164–172 (2018).
- ¹⁸N. E. Grant and J. D. Murphy, "Temporary surface passivation for characterisation of bulk defects in silicon: A review," *Phys. Status Solidi RRL* **11**, 1700243 (2017).
- ¹⁹N. E. Grant, A. I. Pointon, R. Jefferies, D. Hiller, Y. Han, R. Beanland, and J. D. Murphy, "Atomic level termination for passivation and functionalisation of silicon surfaces," *Nanoscale* **12**, 17332–17341 (2020).
- ²⁰T. Niewelt, B. Steinhauser, A. Richter, B. Veith-Wolf, A. Fell, B. Hammann, N. E. Grant, L. Black, J. Tan, A. Youssef, J. D. Murphy, J. Schmidt, M. C. Schubert, and S. W. Glunz, "Reassessment of the intrinsic bulk recombination in crystalline silicon," *Sol. Energy Mater. Sol. Cells* **235**, 111467 (2022).
- ²¹A. I. Pointon, N. E. Grant, S. L. Pain, J. T. White, and J. D. Murphy, "Sub-2 cm²/passivation of silicon surfaces by aprotic solutions," *Appl. Phys. Lett.* **116**, 121601 (2020).
- ²²B. Michl, J. A. Giesecke, W. Warta, and M. C. Schubert, "Separation of front and backside surface recombination by photoluminescence imaging on both wafer sides," *IEEE J. Photovolt.* **2**, 348–351 (2012).
- ²³J. D. Murphy, K. Bothe, R. Krain, V. V. Voronkov, and R. J. Falster, "Parameterisation of injection-dependent lifetime measurements in semiconductors in terms of Shockley-Read-Hall statistics: An application to oxide precipitates in silicon," *J. Appl. Phys.* **111**, 113709 (2012).
- ²⁴D. Stievenard and D. Vuillaume, "Profiling of defects using deep level transient spectroscopy," *J. Appl. Phys.* **60**, 973–979 (1986).
- ²⁵L. C. Kimerling and J. L. Benton, "Oxygen-related donor states in silicon," *Appl. Phys. Lett.* **39**, 410–412 (1981).
- ²⁶A. Chantre, "Metastable thermal donor states in silicon," *Appl. Phys. Lett.* **50**, 1500–1502 (1987).
- ²⁷A. Borghesi, B. Pivac, A. Sassella, and A. Stella, "Oxygen precipitation in silicon," *J. Appl. Phys.* **77**, 4169–4244 (1995).
- ²⁸R. C. Newman, "Oxygen diffusion and precipitation in Czochralski silicon," *J. Phys.: Condens. Matter* **12**, R335–R365 (2000).
- ²⁹K. Hoshi, N. Isawa, T. Suzuki, and Y. Ohkubo, "Czochralski silicon crystals grown in a transverse magnetic field," *J. Electrochem. Soc.* **132**, 693–700 (1985).
- ³⁰C. S. Fuller and R. A. Logan, "Effect of heat treatment upon the electrical properties of silicon crystals," *J. Appl. Phys.* **28**, 1427–1436 (1957).
- ³¹N. E. Grant, P. P. Altermatt, T. Niewelt, R. Post, W. Kwapił, M. C. Schubert, and J. D. Murphy, "Gallium-doped silicon for high-efficiency commercial passivated emitter and rear solar cells," *Solar RRL* **5**, 2000754 (2021).
- ³²S. J. Blundell, "Spin-polarized muons in condensed matter physics," *Contemp. Phys.* **40**, 175–192 (1999).
- ³³A. Hallén, N. Keskitalo, F. Masszi, and V. Nágl, "Lifetime in proton irradiated silicon," *J. Appl. Phys.* **79**, 3906–3914 (1996).
- ³⁴A. O. Ewwaraye and E. Sun, "Electron-irradiation-induced divacancy in lightly doped silicon," *J. Appl. Phys.* **47**, 3776–3780 (1976).
- ³⁵S. D. Brotherton and P. Bradley, "Defect production and lifetime control in electron and γ -irradiated silicon," *J. Appl. Phys.* **53**, 5720–5732 (1982).
- ³⁶B. G. Svensson, B. Mohadjeri, A. Hallén, J. H. Svensson, and J. W. Corbett, "Divacancy acceptor levels in ion-irradiated silicon," *Phys. Rev. B* **43**, 2292–2298 (1991).
- ³⁷J. D. Murphy, A. Wratten, K. Yokoyama, S. L. Pain, A. I. Pointon, N. E. Grant, and J. S. Lord, "Muon spin spectroscopy to probe depth-dependent carrier lifetimes in silicon photovoltaics," *STFC ISIS Neutron and Muon Source* (2021).